Vertical mode expansion method for transmission of light through a single circular hole in a slab

Xun Lu,[1] Hualiang Shi,[1] and Ya Yan Lu[1,*]

[1]*Department of Mathematics, City University of Hong Kong, Kowloon, Hong Kong*

compiled: January 20, 2014

An efficient method is developed for rigorously analyzing the scattering of light by a layered circular cylindrical object in a layered background, and it is applied to study the transmission of light through a subwavelength hole in a metallic film, where the hole may be filled by a dielectric material. The method relies on expanding the electromagnetic field (subtracted by one-dimensional solutions of the layered media) in one dimensional modes, where the expansion "coefficients" are functions satisfying two-dimensional Helmholtz equations. A system of equations is established on the boundary of the circular cylinder to solve the expansion "coefficients". The method effectively reduces the original three-dimensional scattering problem to a two-dimensional problem on the boundary of the cylinder.

OCIS codes: (000.4430) Numerical approximation and analysis; (050.1755) Computational electromagnetic methods.

http://dx.doi.org/10.1364/XX.99.099999

1. Introduction

Transmission of light through a hole in a dielectric slab or a metallic film is a classical problem in electromagnetic theories [1]. The problem has attracted renewed interest due to the discovery of extraordinary optical transmission (EOT) through subwavelength hole arrays or single holes surrounded by surface corrugations in metallic films [2–4]. When the wavelength, the hole size and the slab thickness are on the same order, asymptotic solutions are no longer valid, accurate approximate models are difficult to establish, and a rigorous analysis of the problem can only be obtained by solving the full Maxwell's equations. This is true even when the holes are circular.

General computational electromagentics methods, such as the finite-difference time-domain (FDTD) method [5] and the finite element method (FEM) [6], have been used to study this problem. Although it is extremely popular, FDTD is not very efficient, since it requires a small grid size to resolve interfaces with high index-contrast, a small time step to maintain numerical stability, and proper dispersion models to simulate real metals. Adaptive FEM [7] is very powerful and versatile, but its accuracy may still be limited by the singular field behavior around the hole edges. Surface integral equation method [8, 9] is another choice, but the method is relatively complicated, since it requires the evaluation of many singular integrals. Besides, the integral equations are typically discretized by a low order boundary element method, and the accuracy is often limited by the field singularity along the hole edges. The problem can also be solved by the mode-matching or modal method [10–12] such as the Fourier modal method [13]. In that case, the accuracy depends on the number of eigenmodes used in the expansions. Unfortunately, these two-dimensional (2D) eigenmodes are expensive to compute.

In this paper, we present a relatively simple and efficient method based on expanding the electromagnetic field in one-dimensional (1D) vertical modes, where the slab is assumed to be horizontal, the vertical direction is truncated by perfectly matched layers (PMLs) [14, 15], and the modes are calculated by a Chebyshev pseudospectral method [16]. The vertical modes are eigenmodes of 1D structures and they are different in the two regions corresponding to the hole and the slab. Vertical mode expansions have been used in previous works on photonic crystal slabs [17–20] and microdisk cavities [21], but in these studies, the total field is expanded in the vertical modes directly. For our problem, there is an incident wave in the homogeneous medium above the slab, the total field is not outgoing in the positive vertical direction, and it cannot be expanded in the vertical modes. Instead, the vertical mode expansions are only used after a "one-dimensional" solution is subtracted from the total field. The Chebyshev pseudospectral method [16] is used to find the vertical modes numerically, since it is simple to use, and exhibits high accuracy when applied in a modal method for diffraction gratings [22–24].

Although we emphasize dielectric slabs and metallic

* Corresponding author: mayylu@cityu.edu.hk

films with a single circular hole, our method is applicable to any layered medium with a layered circular cylindrical region. In particular, the slab may be placed on a substrate, the hole may be filled with some material. Instead of holes, we can have a circular cylinder in free space or on a substrate. In the following sections, we present the details of our method and illustrate the method by numerical examples.

2. Problem formulation

We consider a layered structure that contains a circular cylindrical region with a different layer profile, as shown in Fig. 1. In a Cartesian coordinate system $\{x, y, z\}$, the

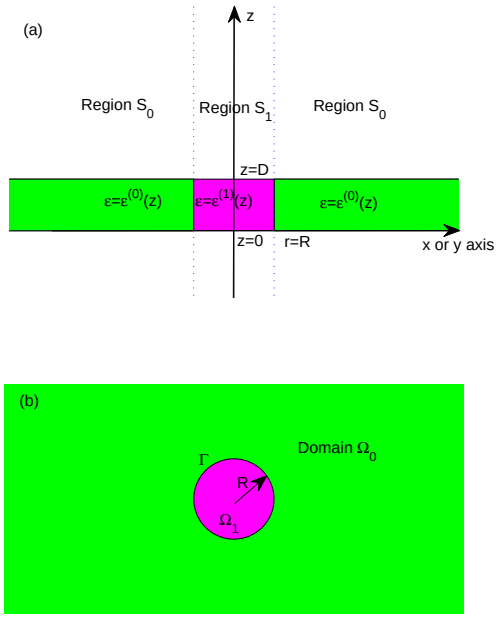

Fig. 1. A circular cylindrical object in a layered background. (a) Vertical cross section in the xz or yz plane; (b) horizontal cross section in the xy plane.

structure is assumed to be parallel to the xy plane and bounded by the planes at $z = 0$ and $z = D$ where D is positive. The media above ($z > D$) and below ($z < 0$) the structure are homogeneous. The circular cylindrical region S_1 is given by $-\infty < z < \infty$ and $r < R$ where $r = \sqrt{x^2 + y^2}$ and R is positive. The region outside the circular cylinder is denoted as S_0 and it is given by $-\infty < z < \infty$ and $r > R$. The cross sections of S_1 and S_0 are 2D domains Ω_1 and Ω_0 in the xy plane, and they are a disk and its exterior, respectively. The common boundary of S_0 and S_1 is the vertical wall W of the cylinder, and its intersection with the xy plane is the circle Γ of radius R.

In terms of the dielectric function ε and relative permeability μ, we assume $\varepsilon = \varepsilon^{(0)}(z)$ and $\mu = \mu^{(0)}(z)$ in S_0, and $\varepsilon = \varepsilon^{(1)}(z)$ and $\mu = \mu^{(1)}(z)$ in S_1, where $\varepsilon^{(0)}$, $\mu^{(0)}$, $\varepsilon^{(1)}$ and $\mu^{(1)}$ are piecewise smooth functions of z. For the homogeneous media above and below the structure, we assume $\varepsilon = \varepsilon_t$ and $\mu = \mu_t$ for $z > D$, and $\varepsilon = \varepsilon_b$ and $\mu = \mu_b$ for $z < 0$, where ε_t, μ_t, ε_b and μ_b are constants. Special examples of such structures are a slab with a circular hole and a circular cylinder on a substrate.

In the medium above the structure ($z > D$), we specify a plane incident wave $\{\mathbf{E}^{(i)}, \mathbf{H}^{(i)}\}$ with a free space wavenumber k_0 and a wave vector $(\alpha, \beta, -\gamma_t)$, where α, β are real and $\gamma_t = (k_0^2\varepsilon_t\mu_t - \alpha^2 - \beta^2)^{1/2}$ is positive. Without the circular region S_1, i.e., for an infinite layered structure, the incident plane wave gives rise to a reflected wave and a transmitted wave in the media above and below the layer. With the circular region S_1, the incident wave also gives rise to a scattered wave that radiates in all directions, and the problem must be solved from the full Maxwell's equations. Assuming the time dependence is $e^{-\mathbf{i}\omega t}$ for an angular frequency ω, the frequency-domain Maxwell's equations are

$$\nabla \times \mathbf{E} = \mathbf{i}k_0\mu\mathbf{H}, \quad \nabla \times \mathbf{H} = -\mathbf{i}k_0\varepsilon\mathbf{E}, \tag{1}$$

where $\mathbf{E}$ is the electric field and $\mathbf{H}$ is the magnetic field multiplied by the free space impedance.

3. One-dimensional solutions

The vertical mode expansions given in latter sections are only valid for electromagnetic fields that are outgoing as $z \to \pm\infty$. The total field $\{\mathbf{E}, \mathbf{H}\}$ is not outgoing in the top region ($z > D$) since it contains an incident wave $\{\mathbf{E}^{(i)}, \mathbf{H}^{(i)}\}$ coming from $z = +\infty$. The incident wave satisfies the Maxwell's equations for $\varepsilon = \varepsilon_t$ and $\mu = \mu_t$. As a result, the difference $\{\mathbf{E} - \mathbf{E}^{(i)}, \mathbf{H} - \mathbf{H}^{(i)}\}$ does not satisfy the homogeneous Maxwell's equations (1). On the other hand, the vertical modes are solutions of the homogeneous Maxwell's equations, therefore, although the field $\{\mathbf{E} - \mathbf{E}^{(i)}, \mathbf{H} - \mathbf{H}^{(i)}\}$ is outgoing, it cannot be expanded in the vertical modes.

Our approach is to subtract a "one-dimensional" solution from the total field, and then expand in the vertical modes. In S_0, the 1D solution $\{\mathbf{E}^{(0)}, \mathbf{H}^{(0)}\}$ is the solution of the Maxwell's equations with the 1D profile $\varepsilon = \varepsilon^{(0)}(z)$, $\mu = \mu^{(0)}(z)$ and the same incident wave. If the original structure is a slab with a circular hole, then $\{\mathbf{E}^{(0)}, \mathbf{H}^{(0)}\}$ is the solution for the slab without the hole. Notice that $\{\mathbf{E} - \mathbf{E}^{(0)}, \mathbf{H} - \mathbf{H}^{(0)}\}$ satisfies the homogeneous Maxwell's equations (1) in S_0, and it is outgoing as $z \to \pm\infty$. For a plane incident wave, the 1D solution $\{\mathbf{E}^{(0)}, \mathbf{H}^{(0)}\}$ is easy to find, since the dependence on x and y can be separated, and the Maxwell's equations are reduced to simple ordinary differential equations. Since the wave vector of the plane incident wave is $(\alpha, \beta, -\gamma_t)$, we have

$$\mathbf{E}^{(0)}(x, y, z) = \tilde{\mathbf{E}}^{(0)}(z)e^{\mathbf{i}(\alpha x + \beta y)},$$
$$\mathbf{H}^{(0)}(x, y, z) = \tilde{\mathbf{H}}^{(0)}(z)e^{\mathbf{i}(\alpha x + \beta y)},$$

and we only need to solve $\tilde{\mathbf{E}}^{(0)}$ and $\tilde{\mathbf{H}}^{(0)}$. In particular, $\{\mathbf{E}^{(0)}, \mathbf{H}^{(0)}\}$ contains a reflected wave with the wave vector $(\alpha, \beta, \gamma_t)$ in the top ($z > D$) and transmitted

wave with wave vector $(\alpha, \beta, -\gamma_b)$ in the bottom ($z < 0$), where $\gamma_b = (k_0^2\varepsilon_b\mu_b - \alpha^2 - \beta^2)^{1/2}$. If $\varepsilon^{(0)}(z)$ and $\mu^{(0)}(z)$ are piecewise constant in z, then $\{\mathbf{E}^{(0)}, \mathbf{H}^{(0)}\}$ can be solved analytically.

In the circular region S_1, we can again find a 1D solution $\{\mathbf{E}^{(1)}, \mathbf{H}^{(1)}\}$ in connection with the layered structure with $\varepsilon = \varepsilon^{(1)}(z)$ and $\mu = \mu^{(1)}(z)$. The difference $\{\mathbf{E} - \mathbf{E}^{(1)}, \mathbf{H} - \mathbf{H}^{(1)}\}$ can then be expanded in vertical modes.

4. Vertical mode expansions

In a layered structure, where μ and ε depend on z only, it is easily shown that the z components of the electromagnetic field satisfy separate three-dimensional (3D) Helmholtz equations:

$$\frac{\partial^2 H_z}{\partial x^2} + \frac{\partial^2 H_z}{\partial y^2} + \frac{\partial}{\partial z}\left[\frac{1}{\mu}\frac{\partial(\mu H_z)}{\partial z}\right] + k_0^2\varepsilon\mu\, H_z = 0, \quad (2)$$

$$\frac{\partial^2 E_z}{\partial x^2} + \frac{\partial^2 E_z}{\partial y^2} + \frac{\partial}{\partial z}\left[\frac{1}{\varepsilon}\frac{\partial(\varepsilon E_z)}{\partial z}\right] + k_0^2\varepsilon\mu\, E_z = 0. \quad (3)$$

A transverse electric (TE) wave is a solution with $E_z = 0$ and $H_z \neq 0$. A solution of Eq. (2) can be obtained by the method of separation of variables. We let

$$\mu H_z(x, y, z) = [\eta^{(e)}]^2\phi^{(e)}(z)V^{(e)}(x, y), \quad (4)$$

where the superscript (e) is used to indicate a TE mode, $\phi^{(e)}$ and $\eta^{(e)}$ satisfy the eigenvalue equation

$$\mu\frac{d}{dz}\left(\frac{1}{\mu}\frac{d\phi^{(e)}}{dz}\right) + k_0^2\varepsilon\mu\,\phi^{(e)} = [\eta^{(e)}]^2\phi^{(e)}, \quad (5)$$

and $V^{(e)}$ satisfies the 2D Helmholtz equation

$$\frac{\partial^2 V^{(e)}}{\partial x^2} + \frac{\partial^2 V^{(e)}}{\partial y^2} + [\eta^{(e)}]^2 V^{(e)} = 0. \quad (6)$$

In Eq. (4), we include the factor $[\eta^{(e)}]^2$ to simplify the expressions for other components of the electromagnetic field. From the Maxwell's equations, it can be shown that the other four components are given by

$$\begin{bmatrix} -E_y \\ E_x \end{bmatrix} = \mathbf{i}k_0\phi^{(e)}\begin{bmatrix} \partial_x V^{(e)} \\ \partial_y V^{(e)} \end{bmatrix},$$

$$\begin{bmatrix} H_x \\ H_y \end{bmatrix} = \frac{1}{\mu}\frac{d\phi^{(e)}}{dz}\begin{bmatrix} \partial_x V^{(e)} \\ \partial_y V^{(e)} \end{bmatrix}.$$

For a smooth curve in the xy plane with a unit normal vector $\boldsymbol{\nu}$ and a unit tangential vector $\boldsymbol{\tau}$ given by

$$\boldsymbol{\nu} = (\nu_x, \nu_y), \quad \boldsymbol{\tau} = (-\nu_y, \nu_x), \quad (7)$$

the tangential field components of the above TE mode are given by

$$E_{\boldsymbol{\tau}} = -\mathbf{i}k_0\phi^{(e)}\frac{\partial V^{(e)}}{\partial \boldsymbol{\nu}}, \quad H_{\boldsymbol{\tau}} = \frac{1}{\mu}\frac{d\phi^{(e)}}{dz}\frac{\partial V^{(e)}}{\partial \boldsymbol{\tau}} \quad (8)$$

where $\partial_{\boldsymbol{\nu}}$ and $\partial_{\boldsymbol{\tau}}$ are the normal and tangential derivative operators.

Similarly, a transverse magnetic (TM) mode is given by

$$H_z = 0, \quad \varepsilon E_z(x, y, z) = [\eta^{(h)}]^2\phi^{(h)}(z)V^{(h)}(x, y), \quad (9)$$

where $\phi^{(h)}$, $\eta^{(h)}$ and $V^{(h)}$ satisfy

$$\varepsilon\frac{d}{dz}\left(\frac{1}{\varepsilon}\frac{d\phi^{(h)}}{dz}\right) + k_0^2\varepsilon\mu\,\phi^{(h)} = [\eta^{(h)}]^2\phi^{(h)}, \quad (10)$$

$$\frac{\partial^2 V^{(h)}}{\partial x^2} + \frac{\partial^2 V^{(h)}}{\partial y^2} + [\eta^{(h)}]^2 V^{(h)} = 0. \quad (11)$$

The superscript (h) is used to indicate a TM mode. The tangential components of the TM mode are given by

$$E_{\boldsymbol{\tau}} = \frac{1}{\varepsilon}\frac{d\phi^{(h)}}{dz}\frac{\partial V^{(h)}}{\partial \boldsymbol{\tau}}, \quad H_{\boldsymbol{\tau}} = \mathbf{i}k_0\phi^{(h)}\frac{\partial V^{(h)}}{\partial \boldsymbol{\nu}}. \quad (12)$$

Since the vertical axis z is unbounded, the layered structure is an open structure which has a continuous spectrum related to the radiation modes. An effective method for avoiding the continuous spectrum is to truncate the top and bottom regions by PML [25, 26]. A PML corresponds to a complex coordinate stretching which replaces z by a complex $\hat{z}$ [15]. In practice, if $d\hat{z} = s(z)dz$ for some function s, then we only need to replace dz in Eqs. (5), (10), (8) and (12) by $s(z)dz$. For our problem, if the PMLs are given in the two intervals $(z_b, \tilde{z}_b)$ and $(\tilde{z}_t, z_t)$ where $\tilde{z}_b \leq 0$ and $\tilde{z}_t \geq D$, then $s(z) \neq 1$ only for $z \in (z_b, \tilde{z}_b)$ and $z \in (\tilde{z}_t, z_t)$. Since the variable z is truncated to the finite interval (z_b, z_t), we can supplement the modified versions of Eqs. (5) and (10) with the following zero boundary conditions

$$\phi^{(p)}(z_b) = \phi^{(p)}(z_t) = 0, \quad p \in \{e, h\}. \quad (13)$$

With the truncation of z by the PMLs, we have discrete sequences of TE and TM modes:

$$\phi_j^{(p)}(z), \quad \eta_j^{(p)}, \quad p \in \{e, h\}, \quad j = 1, 2, 3, ...$$

So far, we have only considered the modes in a general 1D structure. For our problem, there are two 1D structures corresponding to circular region S_1 and its exterior S_0. To distinguish the vertical modes in the two different regions, we add the superscript (1) and (0). Therefore, the vertical modes are denoted as

$$\phi_j^{(l,p)}(z), \quad \eta_j^{(l,p)}, \quad V_j^{(l,p)}(x, y) \quad (14)$$

for $l \in \{0, 1\}$, $p \in \{e, h\}$, and $j = 1, 2, 3, ...$

Based on the vertical TE and TM modes, we can expand the electromagnetic field in the two regions. In S_0, the z components are

$$H_z = H_z^{(0)} + \frac{1}{\mu^{(0)}}\sum_{j=1}^{\infty}[\eta_j^{(0,e)}]^2\phi_j^{(0,e)}\,V_j^{(0,e)} \quad (15)$$

$$E_z = E_z^{(0)} + \frac{1}{\varepsilon^{(0)}}\sum_{j=1}^{\infty}[\eta_j^{(0,h)}]^2\phi_j^{(0,h)}\,V_j^{(0,h)} \quad (16)$$

and tangential components on the vertical wall W of the cylinder ($r = R$) are

$$H_{\boldsymbol{\tau}} = H_{\boldsymbol{\tau}}^{(0)} + \frac{1}{\mu^{(0)}} \sum_{j=1}^{\infty} \frac{d\phi_j^{(0,e)}}{dz} \frac{\partial V_j^{(0,e)}}{\partial \boldsymbol{\tau}} + \mathbf{i}k_0 \sum_{j=1}^{\infty} \phi_j^{(0,h)} \frac{\partial V_j^{(0,h)}}{\partial \boldsymbol{\nu}} \tag{17}$$

$$E_{\boldsymbol{\tau}} = E_{\boldsymbol{\tau}}^{(0)} + \frac{1}{\varepsilon^{(0)}} \sum_{j=1}^{\infty} \frac{d\phi_j^{(0,h)}}{dz} \frac{\partial V_j^{(0,h)}}{\partial \boldsymbol{\tau}} - \mathbf{i}k_0 \sum_{j=1}^{\infty} \phi_j^{(0,e)} \frac{\partial V_j^{(0,e)}}{\partial \boldsymbol{\nu}}. \tag{18}$$

We can also expand the field in the cylinder S_1 and obtain E_z, H_z, $H_{\boldsymbol{\tau}}$, $E_{\boldsymbol{\tau}}$ on the vertical wall W. In the following sections, we present a procedure to calculate the functions $V_j^{(l,p)}$ on the circle Γ.

5. Normal and tangential derivatives

From the previous section, it is clear that the vertical mode expansions involve both normal and tangential derivatives of $V_j^{(l,p)}$ (for $l \in \{0,1\}$, $p \in \{e,h\}$ and positive integers j) along the circle Γ (i.e., at $r = R$), where $V_j^{(l,p)}$ satisfies a Helmholtz equation in Ω_0 (i.e., for $r > R$) or Ω_1 (i.e., for $r < R$) corresponding to $l = 0$ or $l = 1$, respectively. In order to set up a system of equations for solving $V_j^{(l,p)}$ on Γ, we need to approximate the operator $\partial_{\boldsymbol{\tau}}$ and find operators $\Lambda_j^{(l,p)}$ (the so-called Dirichlet-to-Neumann or DtN maps) such that

$$\Lambda_j^{(l,p)} V_j^{(l,p)} = \partial_{\boldsymbol{\nu}} V_j^{(l,p)} \quad \text{on} \quad \Gamma. \tag{19}$$

Notice that all tangential derivatives of $V_j^{(l,p)}$ are associated with the same derivative operator, but the normal derivatives of $V_j^{(l,p)}$ give rise to different operators for different $V_j^{(l,p)}$. This is so because they satisfy different Helmholtz equations. In fact, l is related to the domain where the Helmholtz equation is satisfied, and the coefficient of the equation depends on l, p and j. When the circle Γ is discretized by M points, the operators $\partial_{\boldsymbol{\tau}}$ and $\Lambda_j^{(l,p)}$ are approximated by $M \times M$ matrices.

A matrix approximation to $\partial_{\boldsymbol{\tau}}$ can be easily constructed following the standard Fourier spectral method [16]. Briefly, a function f on Γ can be regarded as a function of θ (where r and θ are the polar coordinates). Given M points of f on the circle, we can constructe an approximate Fourier series of f based on these M points using the discrete Fourier transform, then approximate the derivative of f by the derivative of the Fourier series.

The DtN maps can also be easily constructed based on the general solution of the Helmholtz equation inside or outside the circle Γ. Consider a Helmholtz equation in Ω_0:

$$\partial_x^2 V^{(0)} + \partial_y^2 V^{(0)} + \eta^2 V^{(0)} = 0, \quad r > R. \tag{20}$$

To simplify the notations, we drop the superscripts and subscripts, except for (l) in $V_j^{(l,p)}$. Since $V^{(0)}$ should satisfy the outgoing radiation condition at infinity, the general solution of Eq. (20) is

$$V^{(0)}(r,\theta) = \sum_{m=-\infty}^{\infty} a_m H_m^{(1)}(\eta r) e^{\mathbf{i}m\theta}, \quad r > R, \tag{21}$$

where $H_m^{(1)}$ is the Hankel function of first kind and mth order. The partial derivative of $V^{(0)}$ with respect to r is

$$\partial_r V^{(0)}(r,\theta) = \sum_{m=-\infty}^{\infty} a_m \eta H_m^{(1)\prime}(\eta r) e^{\mathbf{i}m\theta}, \quad r > R, \tag{22}$$

where $H_m^{(1)\prime}$ is the derivative of $H_m^{(1)}$. We can define a linear operator $\Lambda^{(0)}$ satisfying

$$\Lambda^{(0)} e^{\mathbf{i}m\theta} = \lambda_m^{(0)} e^{\mathbf{i}m\theta}, \quad m = 0, \pm 1, \pm 2, ... \tag{23}$$

where

$$\lambda_m^{(0)} = \frac{\eta H_m^{(1)\prime}(\eta R)}{H_m^{(1)}(\eta R)}.$$

Then it is easy to verify that

$$\partial_r V^{(0)} = \Lambda^{(0)} V^{(0)} \quad \text{at} \quad r = R.$$

Since $\partial_r V^{(0)}$ is the normal derivative of $V^{(0)}$ on the circle Γ, $\Lambda^{(0)}$ is the DtN map.

Similarly, for the Helmholtz equation in Ω_1:

$$\partial_x^2 V^{(1)} + \partial_y^2 V^{(1)} + \eta^2 V^{(1)} = 0, \quad r < R, \tag{24}$$

the general solution is

$$V^{(1)}(r,\theta) = \sum_{m=-\infty}^{\infty} b_m J_m(\eta r) e^{\mathbf{i}m\theta}, \quad r < R, \tag{25}$$

and the DtN map $\Lambda^{(1)}$ is the linear operator satisfying

$$\Lambda^{(1)} e^{\mathbf{i}m\theta} = \lambda_m^{(1)} e^{\mathbf{i}m\theta}, \quad m = 0, \pm 1, \pm 2, ..., \tag{26}$$

where

$$\lambda_m^{(1)} = \frac{\eta J_m'(\eta R)}{J_m(\eta R)}.$$

When the circle Γ is discretized by M points, we can find $M \times M$ matrices that approximate the DtN maps. More precisely, if a function f is known at M points on the circle, we can regard f as a function of θ and construct an approximate Fourier series by the discrete Fourier transform, then evaluate $\Lambda^{(0)} f$ by Eq. (23) and $\Lambda^{(1)} f$ by Eq. (26), respectively. This is a linear process and it leads to $M \times M$ matrices.

6. Linear system

To obtain a linear system of equations for $V_j^{(l,p)}$ on the circle Γ, we match the four field components H_z, E_z, $H_{\boldsymbol{\tau}}$ and $E_{\boldsymbol{\tau}}$ on the vertical wall W truncated by PMLs, i.e., at $r = R$ for $z_b < z < z_t$, where z_t and z_b are the endpoints of the PMLs in the top and bottom homogeneous media, respectively. We use a simple collocation scheme where the components are matched at NM points based on M points along the circle and N points in the vertical direction. Let the M points discretizing the circle be $\boldsymbol{r}_1$, $\boldsymbol{r}_2$, ..., $\boldsymbol{r}_M$, and the N points discretizing the vertical direction be z_j for $j = 1, 2, ..., N$, the collocation points are $(\boldsymbol{r}_i, z_j)$ for $1 \le i \le M$ and $1 \le j \le N$. Meanwhile, the differential equations for the TE and TM vertical modes are discretized at the same N points of z, so that for each case the resulting matrix eigenvalue problem involves an $N \times N$ matrix and has exactly N eigenvalues. Therefore, the index j in the vertical mode expansions actually ranges from 1 to N, and the eigenfunctions $\phi_j^{(l,p)}(z)$ are obtained numerically and available only at the N points of z. Furthermore, as described in the previous section, the operators $\partial_{\boldsymbol{\tau}}$ and $\Lambda_j^{(l,p)}$ are approximated by $M \times M$ matrices.

Matching the four field components at these NM points based on the vertical mode expansions in S_0 and S_1, we obtain the following linear system:

$$\begin{bmatrix} A^{(11)} & 0 & A^{(13)} & 0 \\ 0 & A^{(22)} & 0 & A^{(24)} \\ A^{(31)} & A^{(32)} & A^{(33)} & A^{(34)} \\ A^{(41)} & A^{(42)} & A^{(43)} & A^{(44)} \end{bmatrix} \begin{bmatrix} \boldsymbol{x}_1 \\ \boldsymbol{x}_2 \\ \boldsymbol{x}_3 \\ \boldsymbol{x}_4 \end{bmatrix} = \begin{bmatrix} \boldsymbol{b}_1 \\ \boldsymbol{b}_2 \\ \boldsymbol{b}_3 \\ \boldsymbol{b}_4 \end{bmatrix}, \quad (27)$$

where

$$\boldsymbol{x}_1 = \begin{bmatrix} \boldsymbol{v}_1^{(0,e)} \\ \boldsymbol{v}_2^{(0,e)} \\ \vdots \\ \boldsymbol{v}_N^{(0,e)} \end{bmatrix}, \quad \boldsymbol{x}_2 = \begin{bmatrix} \boldsymbol{v}_1^{(0,h)} \\ \boldsymbol{v}_2^{(0,h)} \\ \vdots \\ \boldsymbol{v}_N^{(0,h)} \end{bmatrix},$$

$$\boldsymbol{x}_3 = \begin{bmatrix} \boldsymbol{v}_1^{(1,e)} \\ \boldsymbol{v}_2^{(1,e)} \\ \vdots \\ \boldsymbol{v}_N^{(1,e)} \end{bmatrix}, \quad \boldsymbol{x}_4 = \begin{bmatrix} \boldsymbol{v}_1^{(1,h)} \\ \boldsymbol{v}_2^{(1,h)} \\ \vdots \\ \boldsymbol{v}_N^{(1,h)} \end{bmatrix},$$

and

$$\boldsymbol{v}_j^{(l,p)} = \begin{bmatrix} V_j^{(l,p)}(\boldsymbol{r}_1) \\ V_j^{(l,p)}(\boldsymbol{r}_2) \\ \vdots \\ V_j^{(l,p)}(\boldsymbol{r}_M) \end{bmatrix},$$

for $l \in \{0, 1\}$, $p \in \{e, h\}$, and $j = 1, 2, ..., N$. Since for each j, there are four unknown functions, the above system has $4NM$ unknowns. The coefficient matrix is writen in 4×4 superblocks, where each superblock is an $(NM) \times (NM)$ matrix, or an $N \times N$ block matrix with $M \times M$ blocks. The (i, j) blocks of the superblocks are

$$A_{ij}^{(11)} = \frac{1}{\mu^{(0)}(z_i)} [\eta_j^{(0,e)}]^2 \phi_j^{(0,e)}(z_i) \mathbf{I}$$

$$A_{ij}^{(13)} = -\frac{1}{\mu^{(1)}(z_i)} [\eta_j^{(1,e)}]^2 \phi_j^{(1,e)}(z_i) \mathbf{I}$$

$$A_{ij}^{(22)} = \frac{1}{\varepsilon^{(0)}(z_i)} [\eta_j^{(0,h)}]^2 \phi_j^{(0,h)}(z_i) \mathbf{I}$$

$$A_{ij}^{(24)} = -\frac{1}{\varepsilon^{(1)}(z_i)} [\eta_j^{(1,h)}]^2 \phi_j^{(1,h)}(z_i) \mathbf{I}$$

$$A_{ij}^{(31)} = \frac{1}{\mu^{(0)}(z_i)} \partial_z \phi_j^{(0,e)}(z_i)\, \partial_{\boldsymbol{\tau}}$$

$$A_{ij}^{(32)} = \mathbf{i} k_0 \phi_j^{(0,h)}(z_i)\, \Lambda_j^{(0,h)}$$

$$A_{ij}^{(33)} = -\frac{1}{\mu^{(1)}(z_i)} \partial_z \phi_j^{(1,e)}(z_i)\, \partial_{\boldsymbol{\tau}}$$

$$A_{ij}^{(34)} = -\mathbf{i} k_0 \phi_j^{(1,h)}(z_i)\, \Lambda_j^{(1,h)}$$

$$A_{ij}^{(41)} = -\mathbf{i} k_0 \phi_j^{(0,e)}(z_i)\, \Lambda_j^{(0,e)}$$

$$A_{ij}^{(42)} = \frac{1}{\varepsilon^{(0)}(z_i)} \partial_z \phi_j^{(0,h)}(z_i)\, \partial_{\boldsymbol{\tau}}$$

$$A_{ij}^{(43)} = \mathbf{i} k_0 \phi_j^{(1,e)}(z_i)\, \Lambda_j^{(1,e)}$$

$$A_{ij}^{(44)} = -\frac{1}{\varepsilon^{(1)}(z_i)} \partial_z \phi_j^{(1,h)}(z_i)\, \partial_{\boldsymbol{\tau}},$$

where $\mathbf{I}$ is the $M \times M$ identity matrix, $\partial_{\boldsymbol{\tau}}$ and $\Lambda_j^{(l,p)}$ are understood as their $M \times M$ matrix approximations.

In the right hand side of Eq. (27), the first superblock $\boldsymbol{b}_1$ comes from $H_z^{(1)} - H_z^{(0)}$ at the NM collocation points. It can be written as

$$\boldsymbol{b}_1 = \begin{bmatrix} \boldsymbol{b}_{11} \\ \boldsymbol{b}_{12} \\ \vdots \\ \boldsymbol{b}_{1N} \end{bmatrix},$$

where $\boldsymbol{b}_{1j}$ is a column vector of length M related to z_j. The lth element of $\boldsymbol{b}_{1j}$ is $H_z^{(1)}(\boldsymbol{r}_l, z_j) - H_z^{(0)}(\boldsymbol{r}_l, z_j)$. Since the vertical modes are obtained using PMLs, it is necessary to replace z by $\hat{z}$ in the expressions of $H_z^{(1)}$ and $H_z^{(0)}$, where $\hat{z}$ is the complex variable that defines the PMLs. In the top ($z > D$), the 1D solutions $\{\mathbf{E}^{(l)}, \mathbf{H}^{(l)}\}$ for $l = 0$, 1, are the sums of the incident wave $\{\mathbf{E}^{(i)}, \mathbf{H}^{(i)}\}$ and the reflected waves $\{\mathbf{E}^{(l,r)}, \mathbf{H}^{(l,r)}\}$, but the incident wave is the same for both regions. Therefore, we have

$$H_z^{(1)}(\boldsymbol{r}, z) - H_z^{(0)}(\boldsymbol{r}, z) = H_z^{(1,r)}(\boldsymbol{r}, z) - H_z^{(0,r)}(\boldsymbol{r}, z)$$

for $z > D$. The other three superblocks $\boldsymbol{b}_2$, $\boldsymbol{b}_3$ and $\boldsymbol{b}_4$ are related to $E_z^{(1)} - E_z^{(0)}$, $H_{\boldsymbol{\tau}}^{(1)} - H_{\boldsymbol{\tau}}^{(0)}$, and $E_{\boldsymbol{\tau}}^{(1)} - E_{\boldsymbol{\tau}}^{(0)}$, respectively.

After the functions $V_j^{(l,p)}$ on the circle Γ are solved, it is easy to find $V_j^{(0,p)}$ in Ω_0 and $V_j^{(1,p)}$ in Ω_1 based on the expansions (21) and (25). More precisely, given $V_j^{(l,p)}$ on Γ, we can find the coefficients $\{a_m\}$ or $\{b_m\}$ by discrete Fourier transforms, then the expansions (21) and (25) can be used in domains Ω_0 and Ω_1, respectively.

7. Normalized transmission

For a metallic or dielectric slab with a hole, it is important to calculate the transmitted power through a plane

parallel to the slab in the homogeneous medium below. For a penetrable slab, since the incident wave is a plane wave, the total power transmitted through an infinite plane is infinity, but the extra transmitted power due to the hole is finite. Since the electromagnetic field is available at any point in the truncated domain (the only truncation is in the z direction), this extra transmitted power can be calculated by integrating the z component of the Poynting vector over the entire plane. In the following, we describe an efficient method that requires only line integrals along the curve Γ.

For $z < 0$, we write the total electromagnetic field as

$$\mathbf{E} = \mathbf{E}^{(0)} + \mathbf{E}^{(s)}, \quad \mathbf{H} = \mathbf{H}^{(0)} + \mathbf{H}^{(s)}, \tag{28}$$

where $\{\mathbf{E}^{(0)}, \mathbf{H}^{(0)}\}$ is the 1D solution corresponding to the layered structure in S_0, and $\{\mathbf{E}^{(s)}, \mathbf{H}^{(s)}\}$ is the scattered wave. In the bottom region, $\{\mathbf{E}^{(0)}, \mathbf{H}^{(0)}\}$ is a plane wave propagating towards $z = -\infty$, and it is the transmitted wave for the 1D problem. In S_0 and for $z < 0$, the decomposition (28) corresponds exactly to equations (15)-(18). However, it does not corresponds to a similar set of equations in S_1, since the vertical mode expansions in S_1 are based by the total field subtracted by $\{\mathbf{E}^{(1)}, \mathbf{H}^{(1)}\}$, but our definition of the scattered field is based on the solution $\{\mathbf{E}^{(0)}, \mathbf{H}^{(0)}\}$ in the entire lower half space.

From the decomposition (28), we can re-write the z component of the Poynting vector (with the extra factor of free space impedance due to the scaling of $\mathbf{H}$) as

$$S_z = \frac{1}{2}\mathrm{Re}(E_x\overline{H}_y - E_y\overline{H}_x) = S_z^{(0)} + S_z^{(extra)}, \tag{29}$$

where $\overline{H}_y$ is the complex conjugate of H_y, $S_z^{(0)}$ is the z component of the Poynting vector for $\{\mathbf{E}^{(0)}, \mathbf{H}^{(0)}\}$, and

$$\begin{aligned} S_z^{(extra)} = \frac{1}{2}\mathrm{Re}\Big[&E_x^{(0)}\overline{H}_y^{(s)} - E_y^{(0)}\overline{H}_x^{(s)} + E_x^{(s)}\overline{H}_y^{(0)} \\ &-E_y^{(s)}\overline{H}_x^{(0)} + E_x^{(s)}\overline{H}_y^{(s)} - E_y^{(s)}\overline{H}_x^{(s)}\Big]. \end{aligned} \tag{30}$$

On a plane with a fixed $z < 0$, the power transmitted downwards through an area G is given by $-\int_G S_z d\boldsymbol{r}$. Since $S_z^{(extra)}$ shows up due to the different layered profile in S_1, the extra transmitted power due to the presence of cylindrical structure in S_1 can be defined as

$$P^{(extra)} = -\int_{\mathbb{R}^2} S_z^{(extra)} d\boldsymbol{r}. \tag{31}$$

Notice that the integration is over the entire xy plane (i.e. $\mathbb{R}^2$), and $P^{(extra)}$ is finite since the scattered field decays to zero at infinity. We define the normalized transmission by

$$T = \frac{P^{(extra)}}{P_{\Omega_1}^{(i)}}, \tag{32}$$

where $P_{\Omega_1}^{(i)}$ is the power of the incident wave through a horizontal cross section of the cylindrical region S_1. If $S_z^{(i)}$ is the z component of the Poynting vector for the incident wave, then

$$P_{\Omega_1}^{(i)} = -\int_{\Omega_1} S_z^{(i)} d\boldsymbol{r}$$

for any $z > D$.

For $P^{(extra)}$ in Eq. (31), the integral on the entire xy plane $\mathbb{R}^2$ is the sum of the integrals on Ω_0 and Ω_1, and both of these can be reduced to line integrals on Γ. In Ω_0, the scattered field is given by the vertical mode expansions. For the last two terms in the right hand side of (30), the integral on Ω_0 gives rise to

$$\begin{aligned} I_{jk}^{(0,pp)} &= \int_{\Omega_0} \left[\partial_x V_j^{(0,p)} \partial_x \overline{V}_k^{(0,p)} + \partial_y V_j^{(0,p)} \partial_y \overline{V}_k^{(0,p)}\right] d\boldsymbol{r}, \\ I_{jk}^{(0,pq)} &= \int_{\Omega_0} \left[\partial_x V_j^{(0,p)} \partial_y \overline{V}_k^{(0,q)} - \partial_y V_j^{(0,p)} \partial_x \overline{V}_k^{(0,q)}\right] d\boldsymbol{r}, \end{aligned}$$

where $p, q \in \{e, h\}$, $p \neq q$ and $j, k = 1, 2, ...$ Since $V_j^{(l,p)}$ satisfies a Helmholtz equation in Ω_l, we can use Green's theorem to reduce the above integrals to line integrals on Γ. After some manipulation, we obtain

$$\begin{aligned} I_{jk}^{(0,pp)} &= \frac{1}{\overline{\eta}_k^2 - \eta_j^2} \int_\Gamma \left[\eta_j^2 V_j \overline{\partial_{\boldsymbol{\nu}} V_k} - \overline{\eta}_k^2 \overline{V_k} \partial_{\boldsymbol{\nu}} V_j\right] ds(\boldsymbol{r}), \\ I_{jk}^{(0,pq)} &= \int_\Gamma V_j \overline{\partial_{\boldsymbol{\tau}} V_k}\, ds(\boldsymbol{r}), \end{aligned}$$

where the unit normal vector $\boldsymbol{\nu}$ points into Ω_0, the superscripts $(0,p)$ and $(0,q)$ are dropped for simplicity, and $\eta_j^2 = [\eta_j^{(0,p)}]^2$ is the eigenvalue related to the eigenfunction $V_j^{(0,p)}$, etc. Since we already have the matrix approximations for $\partial_{\boldsymbol{\tau}}$ and the DtN maps, the normal and tangential derivatives of $V_j^{(l,p)}$ on Γ can be easily evaluated. The other terms in (30), as well as the integral on Ω_1, can be similarly reduced to line integrals.

8. Numerical examples

In this section, we present some numerical examples to validate and illustrate our method. The first example is taken from the work of Popov *et al.* [27]. It is a metallic film with a thickness $D = 0.2\,\mu$m, a refractive index $n = 0.52 + 2.88\mathbf{i}$, and a cirular hole of radius $R = 0.125\,\mu$m. The medium below and above the film, and inside the hole, is air. The structure is considered to be non-magnetic, thus $\mu = 1$ everywhere. The coordinates are chosen such that the xy plane is the bottom surface of the film, and the z axis is along the axis of the circular cylindrical hole. In terms of our notations, we have $\varepsilon_t = 1$, $\varepsilon_b = 1$, and $\varepsilon^{(1)}(z) = 1$, $\varepsilon^{(0)}(z) = (0.52 + 2.88\mathbf{i})^2$ for $0 < z < D$. The problem is considered for a normal incident plane wave with a free space wavelength $\lambda = 0.5\,\mu$m and an electric field in the x direction. Thus, $E_x^{(i)} = e^{-\mathbf{i}\gamma_t z}$ where $\gamma_t = k_0 = 2\pi/\lambda = 4\pi\,(\mu\mathrm{m})^{-1}$, and $E_y^{(i)} = E_z^{(i)} = 0$. Popov *et al.* [27] studied this problem using a differential method based on Fourier-Bessel expansions in the

xy plane [28]. The differential method approximates the Maxwell's equations as a system of ordinary differential equations (ODEs) where the unknown functions (functions of z) are the expansion coefficients. If eigenvalue decompositions are used to solve the ODE system, the differential method is identical to a numerical modal method based on the same expansions. In particular, the eigenvalue decompositions are expensive, since they correspond to 2D eigenvalue problems in the xy plane. We use this example to validate our method, since some detailed near field plots are available in [27] and they can be used for comparison.

For this example, we truncate the z axis to (z_b, z_t), where $z_b = -0.25\,\mu$m and $z_t = 0.45\,\mu$m. The PMLs are given in the intervals $(\tilde{z}_t, z_t)$ and $(z_b, \tilde{z}_b)$, where $\tilde{z}_t = 0.25\,\mu$m and $\tilde{z}_b = -0.05\,\mu$m, and the PML function $s(z)$ is defined as

$$s(z) = \begin{cases} 1 + S_t \left[(z - \tilde{z}_t)/(z_t - \tilde{z}_t)\right]^3, & z > \tilde{z}_t, \\ 1, & \tilde{z}_b < z < \tilde{z}_t, \\ 1 + S_b \left[(z - \tilde{z}_b)/(z_b - \tilde{z}_b)\right]^3, & z < \tilde{z}_b, \end{cases} \tag{33}$$

where $S_t = S_b = 5 + 10\mathbf{i}$. The interval (z_b, z_t) is discretized separately in five subintervals $(z_b, \tilde{z}_b)$, $(\tilde{z}_b, 0)$, $(0, D)$, $(D, \tilde{z}_t)$ and $(\tilde{z}_t, z_t)$ using 27, 9, 19, 9 and 27 interior Chebyshev points, respectively [16, 22], so that the total number of discretization ponts for z is $N = 91$. The circle Γ is discretized uniformly by $M = 12$ points, therefore, the linear system (27) has $4NM = 4368$ unknowns. In Fig. 2, we show 2D contour plots for the magnitudes of the total field components E_z and H_z at $z = -1.2236\,$nm (a discretization point below the bottom interface). In Fig. 3, we show $|E_z|$ along the x-axis and $|E_x|$ along both x and y axes, for $z = -1.2236\,$nm. Due to the chosen polarization of the incident field and the symmetry of the structure, we have $E_y = 0$ along both x and y axes and $E_z = 0$ along the y-axis for all z. In general, our numerical results are in good agreement with those of Popov *et al.* [27], but some differences are noticeable. For E_z, our contours in Fig. 2 are smooth, but the contours in [27] have some wiggles. This may be caused by the truncation of Fourier-Bessel expansions in their computation. For $|E_z|$ and $|E_x|$ along the x-axis, the plots in [27] show some oscillations inside the hole and around the interface. According to the authors of [27], these oscillations are due to the Gibbs phenomenon.

The transmission of light through a single subwavelength hole in a metallic film is limited. One way to enhance the transmission is to introduce some surface corrugations around the hole [3]. Another approach is to fill the hole with a high index dielectric meterial [29–32]. Olkkonen *et al.* [31] analyzed the transmission of light through of single circular hole in a silver film, for different film thickness D, and for different dielectric material (of refractive index n_c) filling the hole. They assumed that the media above and below the film is air, the incident wave is a normal incident linearly polarized plane wave with a free space wavelength $\lambda = 488\,$nm, and the refractive index of the silver is $n = 0.05 + 3.02\mathbf{i}$. Therefore, $\varepsilon_t = \varepsilon_b = 1$, $\varepsilon^{(1)} = n_c^2$ and $\varepsilon^{(0)} = (0.05 + 3.02\mathbf{i})^2$ for $0 < z < D$, $E_x^{(i)} = e^{-\mathbf{i}\gamma_t z}$, $E_y^{(i)} = E_z^{(i)} = 0$, where $\gamma_t = k_0 = 2\pi/0.488\,(\mu\text{m})^{-1}$. We analyze this problem using our method developed in previous sections. In Fig. 4, we show the dependence of the normalized transmission T (defined in Section 7) on film thickness D, on hole radius R, and on the refractive index n_c of the medium filling the hole. Our results agree qualitatively with those of Olkkonen *et al.* [31]. For example, we are able to confirm the Fabry-Pérot-like behavior for T versus the film thickness D in Fig. 4(a). However, there are some differences in the actual values of T. For the results shown in Fig. 4, we truncate the z variable and use PMLs with the following parameters: $z_b = -0.25\,\mu$m, $\tilde{z}_b = -0.05\,\mu$m, $\tilde{z}_t = D + 0.05\,\mu$m, $z_t = D + 0.25\,\mu$m, and $S_t = S_b = 32 + 10\mathbf{i}$. We discretize the circle Γ by $M = 12$ points, and discretize the subintervals $(z_b, \tilde{z}_b)$, $(\tilde{z}_b, 0)$, $(0, D)$, $(D, \tilde{z}_t)$ and $(\tilde{z}_t, z_t)$ by 39, 35, 39, 35 and 39 points, respectively. Therefore, the total number of discretization points for z is $N = 187$, and the final lin-

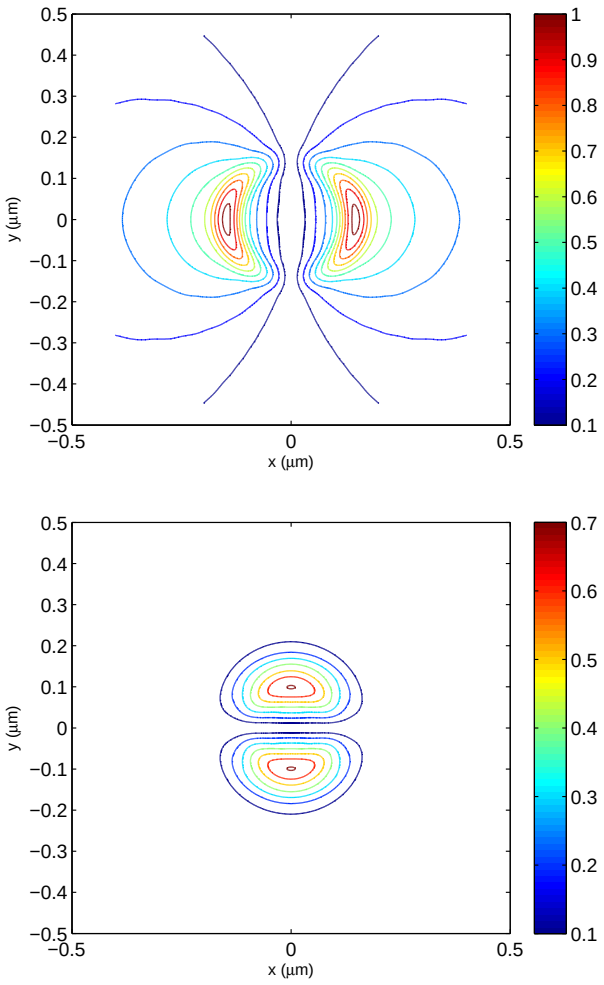

Fig. 2. Contour plots of $|E_z|$ (top panel) and $|H_z|$ (bottom panel) at $z = -1.2236\,$nm.

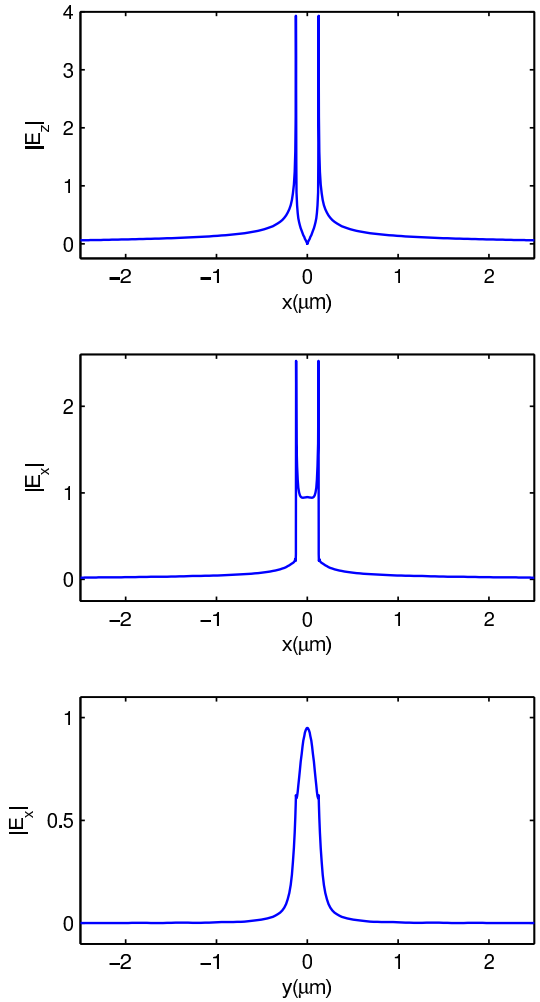

Fig. 3. $|E_z|$ along the x-axis and $|E_x|$ along both x and y axes, for $z = -1.2236\,\text{nm}$.

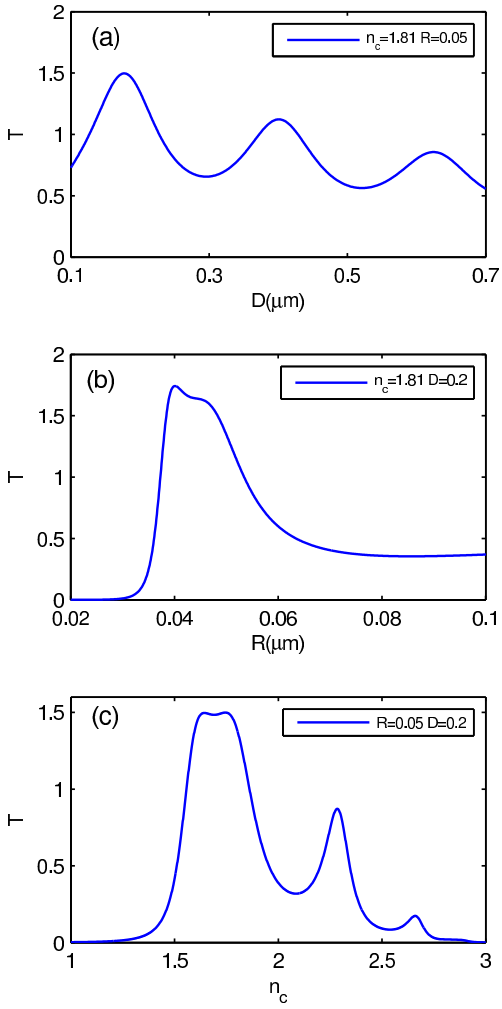

Fig. 4. Normalized transmission T for a silver film with a circular hole filled with a dielectric medium of refractive index n_c. (a) T versus film thickness D for hole radius $R = 50\,\text{nm}$ and $n_c = 1.81$; (b) T versus R for $D = 200\,\text{nm}$ and $n_c = 1.81$, (c) T versus n_c for $D = 200\,\text{nm}$ and $R = 25\,\text{nm}$.

ear system has $4NM = 8976$ unknowns.

9. Conclusions

In the previous sections, we developed a rigorous method for computing the scattering of light by a layered circular cylindrical object in a layered background, and applied the method to metallic films with a circular hole which may be filled by a dielectric material. The 1D vertical modes are calculated numerically by a Chebyshev pseudospectral method [16, 22]. Since PMLs are used to terminate the vertical axis in the computation process, these modes can only represent fields that are outgoing in the vertical direction. Since the total field is not outgoing, the vertical mode expansions are only applied to the difference between the total field and 1D solutions for the layered media. The expansion "coefficients" are functions of x and y satisfying 2D Helmholtz equations, and they are solved from a linear system established on the boundary of the cylinder using the continuity of tangential field components. The method effectively reduces the original 3D scattering problem to a 2D problem. It is relatively simple to implement and is efficient when the vertical structure is simple.

Acknowledgments

This research was partially supported by the Research Grants Council of Hong Kong Special Administrative Region, China (Project No. CityU 102411).

References

[1] M. Born and E. Wolf, Principle of Optics, 7th edition, (Cambridge University Press, 1999).

[2] T. W. Ebbesen, H. J. Lezec, G. F. Ghaemi, T. Thio, and P. A. Wolff, "Extraordinary optical transmission through sub-wavelength hole arrays," Nature **391**, 667-669 (1998).

[3] T. Thio, K. M. Pellerin, R. A. Linke, H. J. Lezec, and T. W. Ebbesen, "Enhanced light transmission through a single subwavelength aperture," Opt. Lett. **26**, 1972-1974 (2001).

[4] F. J. García-Vidal, L. Martin-Moreno, T. W. Ebbesen, and L. Kuipers, "Light passing through subwavelength apertures," Rev. Mod. Phys. **82**, 729–787 (2010).

[5] A. Taflove and S. C. Hagness, Computational Electrodynamics: the finite-difference time-domain method, 2nd ed. (Artech House, 2000).

[6] J. M. Jin, The Finite Element Method in Electromagnetics, 2nd ed., (John Wiley & Sons, 2002).

[7] G. Bao, Z. M. Chen, and H. J. Wu, "Adaptive finite-element method for diffraction gratings," J. Opt. Soc. Am. A **22**, 1106-1114 (2005).

[8] W. C. Chew, M. S. Tong, and B. Hu, Integral Equation Methods for Electromagnetic and Elastic Waves, (Morgan & Claypool, 2009).

[9] J.-C. Nédélec, Acoustic and Electromagnetic Equations: Integral Representations for Harmonic Problems, (Springer, 2001).

[10] J. Mu and W. P. Huang, "Simulation of three-dimensional waveguide discontinuities by a full-vector mode-matching method based on finite-difference schemes," Opt. Express **16**, 18152-18163 (2008).

[11] R. Wang, L. Han, J. Mu, and W. P. Huang, "Simulation of waveguide crossings and corners with complex mode-matching method," J. Lightw. Technol. **30**, 1795-1801 (2012).

[12] W. P. Huang, L. Han, J. Mu, "A rigorous circuit model for simulation of large-scale photonic integrated circuits," IEEE Photonics Journal **4**, 1622-1638 (2012).

[13] E. Silberstein, P. Lalanne, J.-P. Hugonin, and Q. Cao, "Use of grating theories in integrated optics," J. Opt. Soc. Am. A **18**, 2865-2875 (2001).

[14] J. P. Berenger, "A perfectly matched layer for the absorption of electromagnetic waves," J. Comput. Phys. **114**, 185-200 (1994).

[15] W. C. Chew and W. H. Weedon, "A 3D perfectly matched medium from modified Maxwells equations with stretched coordinates," Microwave and Optical Technology Letters **7**, 599-604 (1994).

[16] L. N. Trefethen, Spectral Methods in MATLAB, (Society for Industrial and Applied Mathematics, 2000).

[17] S. Boscolo and M. Midrio, "Three-dimensional multiple-scattering technique for the analysis of photonic-crystal slabs," J. Lightw. Technol. **22**, 2778-2786 (2004).

[18] D. Pissoort, E. Michielssen, D. V. Ginste, and F. Olyslager, "Fast-multipole analysis of electromagnetic scattering by photonic crystal slabs," J. Lightw. Technol. **25**, 2847-2863 (2007).

[19] L. Yuan and Y. Y. Lu, "Dirichlet-to-Neumann map method for analyzing hole arrays in a slab," J. Opt. Soc. Am. B **27**, 2568-2579 (2010).

[20] L. Yuan and Y. Y. Lu, "An efficient numerical method for analyzing photonic crystal slab waveguides," J. Opt. Soc. Am. B**28**, 2265-2270 (2011).

[21] R. P. Wang and M.-M. Dumitrescu, "Theory of optical modes in semiconductor microdisk lasers," J. Appl. Phys. **81**, 3391-3397 (1997).

[22] D. Song, L. Yuan and Y. Y. Lu, "Fourier-matching pseudospectral modal method for diffraction gratings," J. Opt. Soc. Am. A **28**, 613-620 (2011).

[23] G. Granet, "Fourier-matching pseudospectral modal method for diffraction gratings: comment," J. Opt. Soc. Am. A **29**, 1843-1845 (2012).

[24] D. Song and Y. Y. Lu, "Pseudospectral modal method for conical diffraction of gratings," J. Mod. Opt. DOI: 10.1080/09500340.2013.856484 (2013).

[25] H. Derudder, D. De Zutter, and F. Olyslager, "Analysis of waveguide discontinuities using perfectly matched layers," Electronics Letters **34**(22), 2138-2140 (1998).

[26] F. Olyslager, "Discretization of continuous spectra based on perfectly matched layers," SIAM Journal on Applied Mathematics **64**(4), 1408-1433 (2004).

[27] E. Popov, N. Bonod, M. Nevière, H. Rigneault, P.-F. Lenne, and P. Chaumet, "Surface plasmon excitation on a single subwavelength hole in a metallic sheet," Applied Optics **44**, 2332-2337 (2005).

[28] N. Bonod, E. Popov, and M. Nivière, "Differential theory of diffraction by finite cylindrical objects," J. Opt. Soc. Am. A **22**, 481-490 (2005).

[29] F. J. Garcia de Abajo, "Light transmission through a single cylindrical hole in a metallic film," Opt. Express **10**, 1475-1484 (2002).

[30] F. J. García-Vidal, E. Moreno, J. A. Porto, and L. Martín-Morento, "Transmission of light through a single rectangular hole," Phys. Rev. Lett. **95**, 103901 (2005).

[31] J. Olkkonen, K. Kataja, and D. Howe, "Light transmission through a high index dielectric-filled subwavelength hole in a metal film," Opt. Express **13**, 6980-6989 (2005).

[32] H. Xu, P. Zhu, H. G. Craighead, and W. W. Webb, "Resonantly enhanced transmission of light through subwavelength apertures with dielectric filling," Opt. Commun. **282**, 1467-1471 (2009).